PERGAMON

Acta mater. 48 (2000) 3311–3326

Acta MATERIALIA

www.elsevier.com/locate/actamat

COMPRESSIVE RESPONSE OF NiTi SINGLE CRYSTALS

H. SEHITOGLU[1]†, I. KARAMAN[1], R. ANDERSON[1], X. ZHANG[1], K. GALL[2], H. J. MAIER[3] and Y. CHUMLYAKOV[4]

[1]University of Illinois, Department of Mechanical and Industrial Engineering, 1206 W. Green St, Urbana, IL 61801, USA, [2]Department of Mechanical Engineering, University of Colorado, Boulder, CO 80309, USA, [3]University of Paderborn, Lehrstuhl für Werkstoffkunde, D-33095 Paderborn, Germany and [4]Siberian Physical-Technical Institute, Revolution Sq. 1, Tomsk 634050, Russia

(Received 28 January 2000; received in revised form 19 May 2000; accepted 19 May 2000)

Abstract—The deformation of NiTi shape memory single crystals are reported under compression loading for selected crystal orientations and two different Ti_3Ni_4 precipitate sizes. For the [148] orientation, selected for highest recoverable strains, the peak aging treatment decreased the transformation stress from austenite to martensite. At the same time, peak aging raised the flow stress of both the austenite and martensite compared to the overaged case by increasing the resistance of the material to dislocation motion. The transformation proceeds beyond the stress plateau region and extends until martensite yielding occurs. This results in recoverable strain levels equivalent to the theoretical estimate of 6.4%. The [112] orientation was chosen to produce two variant formations and in this case, the transformation proceeded over an ascending stress–strain curve compared to the nearly plateau response for the [148] case. Since the austenite and martensite yield levels are reached at a smaller strain level in this case, the maximum recoverable strain was limited to 3.5% even though the theoretical estimates are near 5.1%. The theoretical estimates of transformation strains were established for Type I and Type II twinning cases to cover all possible habit plane and twin systems. TEM investigations support that slip in austenite occurs concomitant with increasing transformation strains. In the [001] orientation, the unfavorable slip systems for dislocation motion in the austenite inhibit slip and permit recoverable strains similar to the theoretical estimates (nearly 4.2%). The [001] orientation exhibits a continuous increase of flow stress with temperature beyond 360 K unlike any other orientation. The results point out that in order to optimize the material performance, close attention must be paid to the selection of the crystallographic orientation, and the precipitate size through heat treatment.

Keywords: Shape memory; Ni–Ti alloys; Single crystal; Phase transformations

1. INTRODUCTION

The Nitinol (NiTi) alloys are the most widely used shape memory alloys (SMAs) with superior mechanical properties compared to Cu- and Fe-based SMAs [1]. These alloys are often used in aged condition because aging increases the M_s temperature (martensite start temperature) and also raises the slip resistance of austenite and martensite phases while it lowers the critical stress required for transformation from the austenite to martensite. A clear understanding of the role of precipitates has not emerged and the present work is aimed at fulfilling this need.

Both peak aging and overaging treatments have been considered in this study, which produce coherent and semi-coherent Ti_3Ni_4 precipitates in NiTi, respectively. In the aged specimens, recoverable strains for [148], [112], [100] and [111] orientations are determined experimentally and discussed in view of the theoretical estimates. The theoretical results are based on the Phenomenological Theory of Martensite Transformation [2, 3], the Lattice Deformation Theory [4] and the Energy Minimization Theory [5]. More focus is placed on the "Energy Minimization Theory" because it permits the evaluation of multiple twin types (Types I and II). Type I twinning refers to a twin plane with rational indices, while Type II twinning has an irrational twin plane normal. The theoretical estimates represent an upper bound on the transformation (recoverable) strain levels as the yielding of austenite and martensite phases curtail the recoverability. To thoroughly test the orientation dependence of the models, several orientations of single crystals of NiTi were chosen. The [148] orientation represents a crystal orientation with near maximum recoverable strain in compression and the highest resolved shear stress factor

† To whom all correspondence should be addressed.

PII: S1359-6454(00)00153-1

(RSSF) of 0.513, while [112], [100] and [111] represent lower RSSF factors (0.44, 0.39 and 0.25, respectively).

The critical stress levels (0.002 strain offset), and the critical resolved shear stress (CRSS), required to trigger the transformation for different orientations, are also determined in the present work. The lowering of CRSS in the peak-aged samples is partially due to the strong local stress field generated by the coherent Ti_3Ni_4 [6, 7] precipitates and also to the lowering of the Ni concentration in the matrix. Previous experiments [8] on NiTi single crystals have been confined to moderate strain levels tension and compression loadings ($<5\%$). Hence, the martensite yielding regime was not reached. All the experiments in this study are conducted under large strain compression (of the order of 9%) to closely study the interaction between martensite transformation and slip of austenite and martensite domains. Previous work [8] has not considered incremental cycling and did not study the evolution of recoverable strains with deformation. In our previous work [8] the focus was on orientations [001], [110], and [111]. In this work we consider [112] and [148] as well. The aging treatments in the previous work (673 K, 1.5 h and 773 K, 15 h) are also different than the aging treatments in this work.

The strains in compression were incrementally increased to 9% (with nearly 1% increments) with unloading to zero stress after each cycle. Since strains as large as 9% in compression were explored the samples underwent nearly 10 cycles. First, elastic deformation of the austenite, and then transformation to martensite occurred. We make the interesting observation that the recoverable strains continue to increase during Stage II, which is the region of deformation above the transformation stress and extends to the martensite yield stress. Once martensite yielding occurred the recoverable strains decreased with further straining. Because the experiments were conducted under cyclic loading conditions, considerable strengthening was observed when multiple variants or slip systems were activated. As the local pile up of dislocations become pronounced, the transformation slope increased dramatically, and the plateau region characteristic of transformation disappeared. Because of the presence of precipitates, the transformation is highly nonhomogenous with untransformed regions around precipitates [6–10] and also localized slip near precipitates. With increasing number of cycles, the slip deformation at the precipitates accumulates, which in turn limits the reversibility of the transformation. Due to the internal stresses, the reversed stress–strain behavior is highly non-linear. Only when the alloy is deformed to large strains and the deformation becomes homogenous, a more distinct reversed transformation stress can be identified. Also, orientations that lie on the symmetry boundary ([111], [001] and [112]) have more than one favorable martensite plate, while the orientation [148] inside the stereographic triangle produces a single martensite plate. The strain hardening is expected to be higher for the symmetric orientations consistent with experimental findings.

Because the experiments were conducted under compression, it was possible to study the yielding of the martensite at high strains following austenite to martensite transformation. The Schmid factors for yielding of the austenitic and martensitic phases were determined and utilized for interpretation of the experimental results. The results also confirm that the martensite yield levels are higher for the case of peak-aged coherent precipitates compared to the over-aged case. A key finding is that large transformation strains can only be realized if the critical stress for both austenite and martensite slip is much higher than the austenite to martensite transformation stress.

The aging treatments studied in this work differ compared to the previous work of the authors [6–9]. The work includes complete Clasius–Clapeyron curves (approximately 80 tests) and the austenite yield behavior for all four crystal orientations, two aging treatments with experiments in the temperature range 200–440 K. These results will clearly show that [001] crystal orientation exhibits an increased flow stress with increasing temperature beyond the pseudoelasticity regime.

2. EXPERIMENTAL PROCEDURE

Single crystal Ti–50.8at.%Ni samples were prepared from a single material batch. The single crystal samples were grown by the Bridgman technique in an inert gas atmosphere. The orientation of single crystal specimens was determined by using electron back-scatter diffraction patterns. Solutionizing of the specimens was conducted at

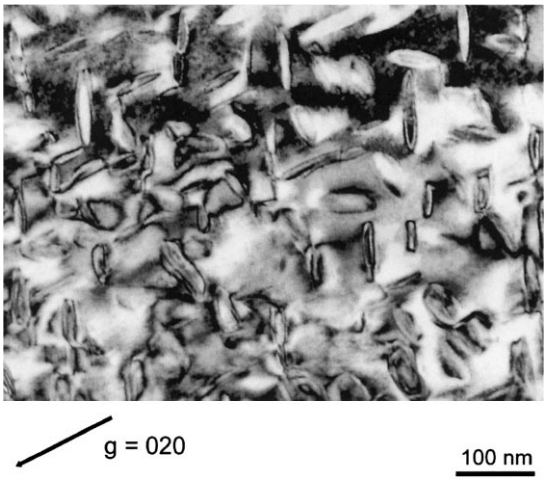

Fig. 1. Two beam bright-field TEM micrograph of NiTi specimen oriented in [148] direction in the peak-aged condition.

1273 K for 2 h in an inert gas atmosphere. Then, one set of specimens were aged at 723 K for 1.5 h and another set of specimens were aged at 823 K for 1.5 h. The first treatment is termed as the "peak-aged" treatment, while the second treatment is the "over-aged" treatment. A Perkins-Elmer differential scanning calorimeter (DSC) was used to determine the transformation temperatures. The DSC analysis shows that the austenite start temperature, A_s, for over-aged and peak-aged samples are 280 K and 288 K, respectively, while the M_s, martensite start temperature, is approximately the same and equals 240 K. The peak-aged and over-aged microstructures are shown in Figs 1 and 2, respectively. In the peak-aged case the average precipitate size is 90 nm while in the over-aged case it is 300 nm.

The specimen cross-section was square, 4 mm wide and 8 mm high. In the experiments, the loads were measured with a load cell, and strains were measured with a miniature MTS (Materials Test Systems) extensometer with 3 mm gage length. The use of the miniature extensometer circumvents the end effects associated with stroke measurements.

To gain insight into the results, the critical stress for transformation as a function of temperature has been determined with a series of deformation experiments. The results are summarized in Figs 3 and 4. In Fig. 3 the results are shown for the over-aged treatment, while in Fig. 4 the results are given for the peak-aged case. The M_s is obtained by extrapolation of the stress–temperature relation to zero stress as 240 K. The slope of the stress-temperature relation in the pseudoelasticity regime is linear and this region is described with the Clausius–Clapeyron relation [1]. The slope of the Clasius–Clapeyron curve ($A \rightarrow M$ region) is in the range 4–8 MPa/°C depending on the crystal orientation. The results also show the magnitudes of stress required

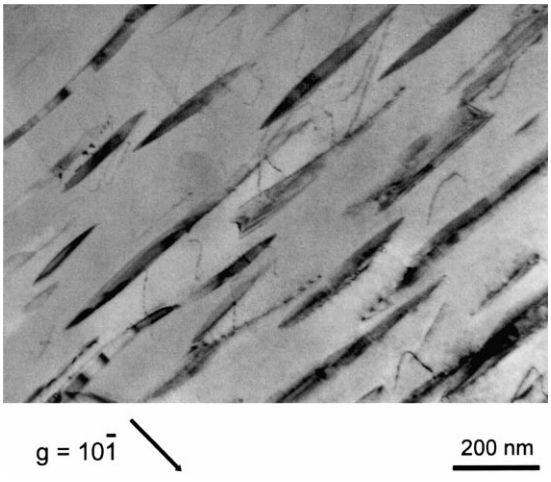

Fig. 2. Two-beam bright-field TEM micrograph showing the microstructure of a [112] oriented NiTi specimen in over-aged condition.

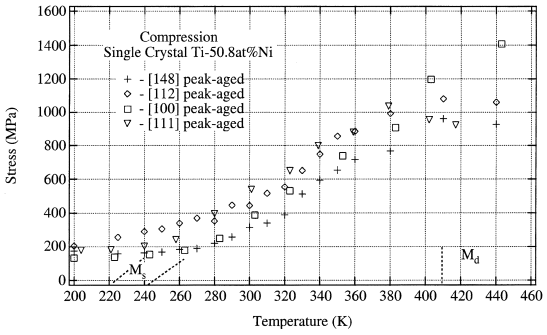

Fig. 3. Transformation stress (0.2% offset) as a function of temperature; over-aged case.

for austenite slip, the martensite deformation and reorientation region ($M \rightarrow M$, martensite to martensite) and the M_d temperature. The M_d temperature is the transition temperature from the Clasius–Clapeyron curve to austenite slip; it is defined as the maximum temperature below which pseudoelastic deformation occurs. Note that the M_d temperature is higher for the peak-aged case. The most significant finding from these experiments is that for the [001] orientation the yield stress continues to increase with temperature and slip deformation is curtailed. Theoretically, the austenite yield stress corresponds to cleavage stress of the material in the [001] direction. In other orientations, it is clear that the peak-aging treatment produces austenite yield levels exceeding 1000 MPa, while the over-aged case produces critical stress levels below 1000 MPa.

3. AUSTENITE TO MARTENSITE TRANSFORMATION

The results of austenite to martensite transformation can be best understood with the aid of Fig. 5. This figure depicts NiTi deformation behavior in compression at temperatures above the austenite start temperature (A_s). Different stages of deformation in shape memory alloys are presented in this figure. After elastic deformation of the austenitic phase (Stage I), a stress-induced martensitic

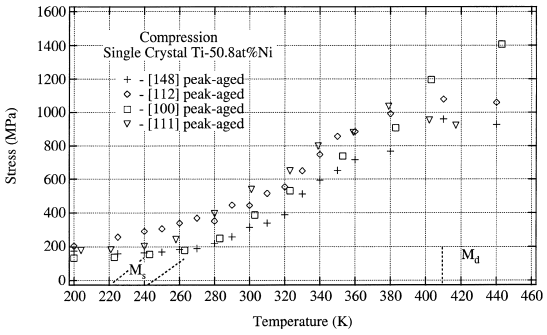

Fig. 4. Transformation stress (0.2% offset) as a function of temperature; peak-aged case.

transformation initiates at a critical stress, $\sigma_{cr}^{A\rightarrow M}$. In Stage II, at small strains, the austenite to martensite transformation occurs ($A \rightarrow M$), at a zero slope or small slope. The transformation slope depends on the number of CVPs (correspondent variant pairs) activated for the single crystal or the texture of the material for polycrystals. A CVP, correspondent variant pair, is a formal term for two twin related martensite variants. During Stage II elastic deformation of the martensite and some slip of austenite initiates at a critical stress level, σ_{cr}^{A}, depending on the crystal orientation and aging treatment. Crystal orientations that are not favorable to slip or fine precipitates produce higher austenite strength levels. The austenite yield stress levels can be ascertained from Figs 3 and 4. If the material is cycled in Stage II, rapid cyclic hardening develops which indicates dislocation activity in the NiTi. We assert that dislocation activity develops in austenite since the critical stress for martensite yielding is 60% higher than the austenite yield strength. This is seen in a later section. When the critical stress for martensite yield, σ_{cr}^{M}, is reached, the stress–strain curve exhibits downward curvature (Stage III). The slip of martensite proceeds until either the specimen fractures or gross deformation occurs.

Upon unloading the martensitic single crystal undergoes elastic deformation (with elastic modulus E_m) followed by pseudo-elastic behavior. In the pseudoelastic regime, reversed transformation (martensite to austenite) occurs. At zero stress, further strain can be recovered upon heating to $A_f + 80$ K where A_f is the austenite finish temperature. If the applied strains were large, inelastic deformation remains at zero stress even after heating and cannot be recovered. The amount of inelastic

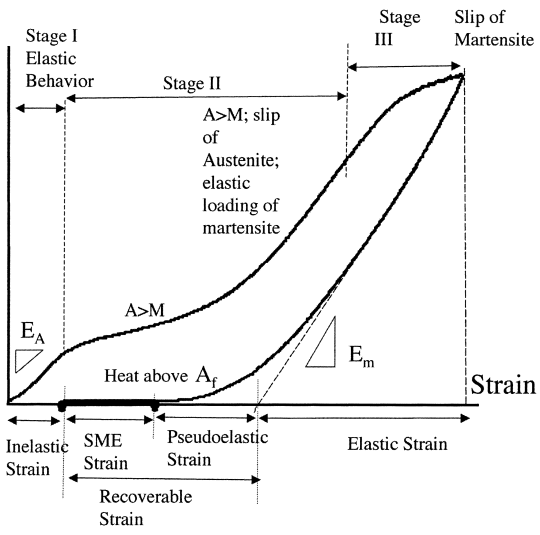

Fig. 5. A schematic of the deformation mechanisms and the strain definitions in single crystals. Deformation is in compression and the test temperature $T > A_s$.

Table 1. The 12 lattice corresponding variants (see Fig. 6 for visualization). The m refers to martensite and p refers to parent (austenite)

Variant	1	2	3	4	5	6	7	8	9	10	11	12
$[100]_m$	$[100]_p$	$[\bar{1}00]_p$	$[100]_p$	$[\bar{1}00]_p$	$[010]_p$	$[0\bar{1}0]_p$	$[010]_p$	$[0\bar{1}0]_p$	$[001]_p$	$[00\bar{1}]_p$	$[001]_p$	$[00\bar{1}]_p$
$[010]_m$	$[011]_p$	$[0\bar{1}1]_p$	$[0\bar{1}1]_p$	$[011]_p$	$[101]_p$	$[\bar{1}01]_p$	$[\bar{1}01]_p$	$[\bar{1}01]_p$	$[\bar{1}10]_p$	$[\bar{1}\bar{1}0]_p$	$[\bar{1}10]_p$	$[\bar{1}\bar{1}0]_p$
$[001]_m$	$[0\bar{1}1]_p$	$[011]_p$	$[011]_p$	$[0\bar{1}1]_p$	$[\bar{1}01]_p$	$[101]_p$	$[\bar{1}01]_p$	$[\bar{1}01]_p$	$[110]_p$	$[\bar{1}10]_p$	$[\bar{1}10]_p$	$[\bar{1}\bar{1}0]_p$

deformation depends on the maximum strain reached in the loading portion of the cycle. The recoverable strain in Fig. 5 is defined as the sum of the pseudoelastic strain and the SME (shape memory effect) strain.

4. CALCULATION OF RECOVERABLE STRAINS

4.1. Phenomenological theory

The orientation dependence of recoverable strains for a single crystal NiTi can be evaluated from the phenomenological theory of martensitic transformations (PTMT) [2, 3]. There are a total of 12 lattice correspondent variants in the cubic to monoclinic transformation of NiTi. These lattice variants are listed in Table 1 as 1–12. The austenite phase is designated as the parent phase. A CVP is a formal term for two twin related martensite variants and stands for "correspondent variant pair" [such as (9, 12)]. A schematic of the variant ♯9 in the parent and martensitic states are shown in Fig. 6. Each martensite CVP is described by a unique habit plane normal, **m**, and transformation shear, **b** (see Fig. 7 for a schematic). In the parent phase coordinate system (B2), the base crystallographic parameters for solutionized NiTi are: $\mathbf{m} = \{-0.8684, 0.2688, 0.4138\}$ and $\mathbf{b}/|\mathbf{b}| = \langle 0.4580, 0.7706, 0.4432\rangle$ [11]. The habit plane solution above is obtained using [011] Type II twinning which is consistent with the dominant mode experimentally observed. In Type II twinning, the twin plane normal is irrational, while in Type I the twin plane normal is rational. The schematic given in Fig. 7 demonstrates the relevant vectors, internally twinned martensite and the single crystal austenite. The vectors **a** and **n** represent the lattice invariant shear (twin shear) and the twin plane, respectively. The shear strain magnitude for the transformation is $|\mathbf{b}| = 0.13$ which is the same for all 24 CVPs.

When the resolved shear stress on the most favorably oriented martensite CVP reaches a critical resolved shear stress, the transformation proceeds on that CVP. Notably, the transformation is unidirectional, so the resolved shear stress must be in the prescribed transformation direction in order to trigger the transformation. The results for [001] and [111] orientations were given in Ref. [8], in this paper we consider [112] and [148] orientations as well.

According to the Buchheit–Wert model [3], the detwinning strain can be added to determine the total transformation strain. Detwinning is the growth of one variant within a CVP at the expense of the other. Under compression, the detwinning strains are typically small but not negligible. We note that the calculations made by Wert assumed small strain formulation, orthogonal **m** and $\mathbf{b}/|\mathbf{b}|$ vectors and Type II-1 twinning cases. We present a more general solution below under the "Energy Minimization Theory".

4.2. Energy minimization theory

The main difference between this theory and the phenomenological theory is that in the phenomenological theory the lattice invariant shear (twinning shear or slip shear) should be known a priori from experimental observations (e.g., this lattice invariant shear was selected as ⟨011⟩ Type II twin for NiTi in phenomenological theory); while in the energy minimization theory no prior assumptions are necessary. The twinning system and the habit planes are an outcome of the solution [5]. Solutions are obtained for both Type I and Type II twinning resulting in a larger number of possible habit planes (192 planes in total). Once the planes are established it is possible to determine the RSSF (resolved shear stress factor) and the recoverable strains associated with the transformation. These results are in agreement

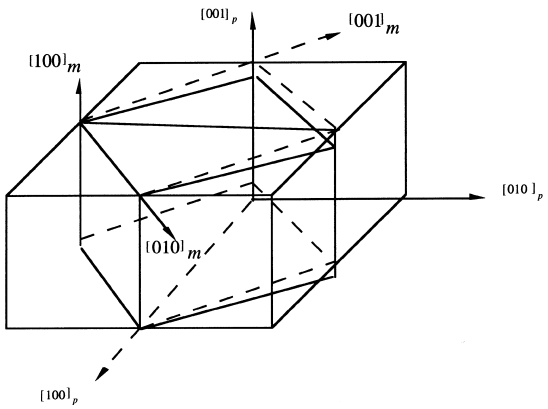

Fig. 6. A schematic description of the variant ♯9.

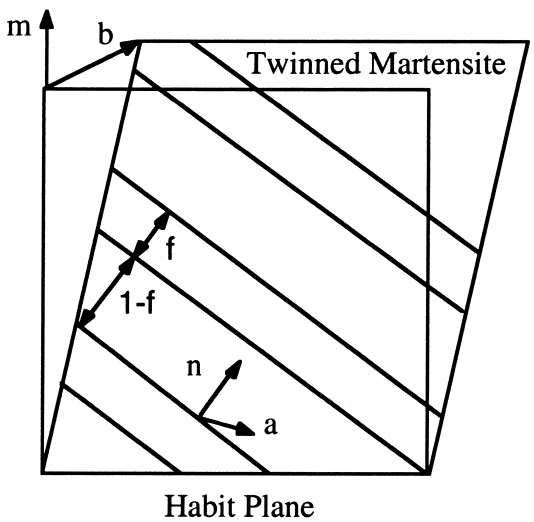

Fig. 7. Twin (**n**) and habit (**m**) planes, and twin shear (**a**) and macroscopic shear (**b**) of martensite.

with the phenomenological theory for ⟨011⟩ Type II twinning with two modifications. The theory was utilized to determine the additional detwinning strain for compression cases and a large strain definition was used in the present work.

We now consider the application of energy minimization theory [5] to NiTi with the extensions noted above. Using the 12 independent lattice correspondences in Table 1, the deformation gradient matrix, **F**, and its symmetric part, **U**, were determined in the cubic reference frame. There are 12 deformation gradient matrices with each one a function of the lattice parameters of the cubic and monoclinic phases. An example of **F** and **U** for variant 1 in Table 1 is:

$$\mathbf{F}_1 = \begin{bmatrix} \alpha & \dfrac{\gamma\ \cos\ \theta}{\sqrt{2}} & \dfrac{\gamma\ \cos\ \theta}{\sqrt{2}} \\ 0 & \dfrac{\beta+\gamma\ \sin\ \theta}{2} & \dfrac{-\beta+\gamma\ \sin\ \theta}{2} \\ 0 & \dfrac{-\beta+\gamma\ \sin\ \theta}{2} & \dfrac{\beta+\gamma\ \sin\ \theta}{2} \end{bmatrix}, \quad \mathbf{U}_1 = \begin{bmatrix} \Delta_1 & \phi & \phi \\ \phi & \Delta_2 & \psi \\ \phi & \psi & \Delta_2 \end{bmatrix} \tag{1}$$

where $\alpha = a/a_0$, $\beta = b/\sqrt{2}a_0$, $\gamma = c/\sqrt{2}a_0$, a_0, a, b, c are, respectively, the lattice parameters of austenite and martensite; θ is the monoclinic angle between b and c in the martensitic lattice; and

$$\Delta_1 = \frac{\alpha^2 + \alpha\gamma\ \sin\ \theta}{\sqrt{\alpha^2+\gamma^2+2\alpha\gamma\ \sin\ \theta}}, \qquad \Delta_2 = \frac{1}{2}\left(\frac{\gamma^2+\alpha\gamma\ \sin\ \theta}{\sqrt{\alpha^2+\gamma^2+2\alpha\gamma\ \sin\ \theta}} + \beta\right), \tag{2}$$

$$\phi = \frac{\alpha\gamma\ \cos\ \theta}{\sqrt{2(\alpha^2+\gamma^2+2\alpha\gamma\ \sin\ \theta)}}, \qquad \psi = \frac{1}{2}\left(\frac{\gamma^2+\alpha\gamma\ \sin\ \theta}{\sqrt{\alpha^2+\gamma^2+2\alpha\gamma\ \sin\ \theta}} - \beta\right) \tag{3}$$

The other independent symmetric transformation strains $\mathbf{U}_2, \ldots, \mathbf{U}_N$ can be generated from $\mathbf{Q}^{\mathrm{T}}\mathbf{U}_1\mathbf{Q}$, where **Q** is one of the 24 rotations in austenite point group (between lattice correspondent variants). The number N equals 12 in the transformation from cubic to monoclinic.

The symmetric deformation gradient matrix **U** can be obtained from the polar decomposition of **F**,

$$\mathbf{F} = \mathbf{R}\cdot\mathbf{U} \tag{4}$$

where **R** represents a rigid body rotation and **U** is the symmetric part of **F**. **U** and **R** can be obtained by

$$\mathbf{U} = \sqrt{\mathbf{F}^{\mathrm{T}}\cdot\mathbf{F}}, \quad \mathbf{R} = \mathbf{F}\cdot\mathbf{U}^{-1} \tag{5}$$

where $\mathbf{F}^{\mathrm{T}}$ is the transpose of **F**.

There are two kinds of invariant (undistorted) plane in the twinned martensite. One is the twin plane (interface between the two lattice correspondence variants), the other is the habit plane [interface between twinned martensite and parent phase (see Fig. 7 for a schematic)]. Using the first condition, the kinematic compatibility between the two correspondence variants in the twin across the twin plane requires

$$\mathbf{R}_{ij}\mathbf{U}_j - \mathbf{U}_i = \mathbf{a}\otimes\mathbf{n} \tag{6}$$

where $\mathbf{U}_i$ and $\mathbf{U}_j$ are two lattice correspondence variants which form the twin, $\mathbf{R}_{ij}$ is an orthogonal tensor (of rank 2) satisfying $\mathbf{R}_{ij}^{\mathrm{T}}\cdot\mathbf{R}_{ij} = \mathbf{I}$ (**I** is second rank identity tensor). The $\mathbf{R}_{ij}$ represents the relative rotation between the two variants, **n** is the twinning plane normal, **a** is the twinning shear direction. The subscript i, j in equation (6) represent different choices of the integers {1, 2, …, 12} and there is no summation of the index. The ⊗ represents a dyadic product. One hundred and thirty-two possible pairs of ($\mathbf{U}_i$, $\mathbf{U}_j$) can be formed from the 12 lattice correspondent variants, so there are 132 equations in equation (6). The unknowns in equation (6) are **a**, **n** and $\mathbf{R}_{ij}$ for a given pair of $\mathbf{U}_i$ and $\mathbf{U}_j$. These values can be obtained as follows [5].

Equation (6) is post-multiplied by $\mathbf{U}_i^{-1}$,

$$\mathbf{R}_{ij}\mathbf{U}_j\mathbf{U}_i^{-1} = \mathbf{I} + \mathbf{a}\otimes(\mathbf{n}\mathbf{U}_i^{-1}) \quad \text{(no summation)} \tag{7}$$

A symmetric matrix **C** is formed as

$$\mathbf{C} = (\mathbf{R}_{ij}\mathbf{U}_j\mathbf{U}_i^{-1})^{\mathrm{T}}\cdot(\mathbf{R}_{ij}\mathbf{U}_j\mathbf{U}_i^{-1}) = \mathbf{U}_i^{-1}\cdot\mathbf{U}_j^2\cdot\mathbf{U}_i^{-1} \tag{8}$$

where the superscript T and 2, respectively, represent the transpose and square of a tensor. The sufficient and necessary condition of equation (6) having solutions is that **C** has ordered eigenvalues of $\lambda_1 \le \lambda_2 = 1 \le \lambda_3$. Under this case, **C** can be written as

$$\mathbf{C} = (\mathbf{I} + \mathbf{n}'\otimes\mathbf{a}')\cdot(\mathbf{I} + \mathbf{a}'\otimes\mathbf{n}') \tag{9}$$

where

$$\mathbf{a}' = \mathbf{a},\ \mathbf{n}' = \mathbf{U}_i^{-1}\cdot\mathbf{n} \tag{10}$$

The vectors $\mathbf{a}'$ and $\mathbf{n}'$ are solved as [5],

$$\mathbf{a}' = \rho\left(\sqrt{\frac{\lambda_3(\lambda_2-\lambda_1)}{\lambda_3-\lambda_1}}\mathbf{e}_1 + \kappa\sqrt{\frac{\lambda_1(\lambda_3-\lambda_2)}{\lambda_3-\lambda_1}}\mathbf{e}_3\right) \tag{11}$$

$$\mathbf{n}' = \rho^{-1}\left(\frac{\sqrt{\lambda_3}-\sqrt{\lambda_1}}{\sqrt{\lambda_3-\lambda_1}}\right)\left(-\sqrt{\lambda_2-\lambda_1}\mathbf{e}_1 + \kappa\sqrt{\lambda_3-\lambda_2}\mathbf{e}_3\right) \tag{12}$$

where $\mathbf{e}_1$, $\mathbf{e}_2$ and $\mathbf{e}_3$ are the three eigenvectors of matrix $\mathbf{C}$ corresponding to λ_1, λ_2 and λ_3, respectively. The constant ρ represents an invariant scaling of the solution and will be used to choose unit normal vector $\mathbf{n}$. The constant κ can take the value ± 1. We denote the solution of $(\mathbf{R}_{ij}, \mathbf{a}, \mathbf{n})$ with $\kappa = +1$ as $(\mathbf{R}_{ij}^{+}, \mathbf{a}^{+}, \mathbf{n}^{+})$ and $\kappa = -1$ as $(\mathbf{R}_{ij}^{-}, \mathbf{a}^{-}, \mathbf{n}^{-})$. The relationship between the twinning elements and $\mathbf{a}$, $\mathbf{n}$ in the parent phase basis are respectively [12],

$$(\mathbf{K}_1^{+}, \eta_1^{+}, \mathbf{K}_2^{+}, \eta_2^{+}) \| (\mathbf{n}^{+}, \mathbf{U}_i^{-1}\mathbf{a}^{+}, \mathbf{n}^{-}, \mathbf{U}_i^{-1}\mathbf{a}^{-})$$

and

$$(\mathbf{K}_1^{-}, \eta_1^{-}, \mathbf{K}_2^{-}, \eta_2^{-}) \| (\mathbf{n}^{-}, \mathbf{U}_i^{-1}\mathbf{a}^{-}, \mathbf{n}^{+}, \mathbf{U}_i^{-1}\mathbf{a}^{+})$$

where $\mathbf{K}_1$ is normal of the first undistorted plane in the twin (usually referred to as twinning plane), $\mathbf{K}_2$ is the normal of the second undistorted plane (or conjugate twinning plane), η_1 is the shear direction which lies in the twinning plane and η_2 another undistorted direction in the $\mathbf{K}_2$ plane.

Substituting the above 132 possible pairs of $(\mathbf{U}_i, \mathbf{U}_j)$ into equation (6), 84 of them yield solutions. Furthermore, only 42 are independent since the pair $(\mathbf{U}_i, \mathbf{U}_j)$ is equivalent to $(\mathbf{U}_j, \mathbf{U}_i)$. For each equation we obtain two solutions because of $\kappa = \pm 1$. Therefore, there are 84 possible twins. These 84 twins can be divided into seven groups as: $\{100\}\langle 011\rangle$ compound twins, $\{100\}\langle 0,\ 0.7864,\ \bar{1}\rangle$ Type I twins, $\{1\ \bar{1}\ 0\}\langle 1\ 1\ 0.3230\rangle$ Type I twins, $\{1\ \bar{1}\ 0\}\langle 1\ 1\ 2.7008\rangle$ Type I twins, $\{0.7205,\ 0,\ \bar{1}\}\langle 010\rangle$ Type II twins, $\{\bar{1},\ 1,\ 0.4953\}\langle 110\rangle$ Type II twins and $\{1,\ 1,\ 3.0495\}\langle \bar{1}10\rangle$ Type II twins. Each group has 12 twins, respectively. Note that all the indexes are presented in parent phase basis.

In the above development, we have determined all the possible twins (number of twins, twin plane normal $\mathbf{n}$ and twinning shear vector $\mathbf{a}$) by using the invariant plane condition of twinning plane. The second invariant plane condition of habit plane will be used to determine the habit plane normal and transformation strain. The kinematic compatibility between the martensite and austenite across the habit plane requires

$$\mathbf{F}_{\mathrm{M}} - \mathbf{I} = \mathbf{b} \otimes \mathbf{m} \tag{13}$$

where $\mathbf{I}$ is the identity tensor, $\mathbf{m}$ is the habit plane normal and $\mathbf{b}$ is the shear of the martensite, and $\mathbf{F}_{\mathrm{M}}$ is the average deformation gradient of the twinned martensite. For a stack of thin twin layers, $\mathbf{F}_{\mathrm{M}}$ satisfies [5],

$$\mathbf{F}_{\mathrm{M}} = \mathbf{R}_{\mathrm{h}}(f\mathbf{R}_{ij}\mathbf{U}_j + (1-f)\mathbf{U}_i) \tag{14}$$

where $\mathbf{U}_i$ and $\mathbf{U}_j$ are the two lattice correspondence variants in the twin, and $(1-f)$ and f are their volume fractions, and $\mathbf{R}_h$ is the relative rotation between the twinned martensite and the parent phase. The $\mathbf{R}_h$ and f are unknown and will be determined as follows. Upon substituting equation (6) and equation (14) into equation (13),

$$\mathbf{R}_h(\mathbf{U}_i + f\mathbf{a} \otimes \mathbf{n}) = \mathbf{I} + \mathbf{b} \otimes \mathbf{m} \tag{15}$$

There are 84 equations in equation (15) since there are 84 possible pairs of $(\mathbf{a}, \mathbf{n})$. Following the procedure of solving equation (6), we form matrix $\mathbf{C}(f)$ as

$$\mathbf{C}(f) = (\mathbf{U}_i + f\mathbf{n} \otimes \mathbf{a})(\mathbf{U}_i + f\mathbf{a} \otimes \mathbf{n}) \tag{16}$$

Again the sufficient and necessary condition for equation (15) having solutions is that $\mathbf{C}(f)$ has ordered eigenvalues of $\lambda_1 \le \lambda_2 = 1 \le \lambda_3$. So the volume fraction f can be obtained by

$$\det(\mathbf{C}(f) - \mathbf{I}) = 0 \tag{17}$$

where $\det(\cdot)$ is the determinant of a matrix. Substituting the above 84 possible twins into equations (16) and (17), the following four groups of twins have solutions of f and ordered eigenvalues of $\lambda_1 \le \lambda_2 = 1 \le \lambda_3$: Type I-1$\{100\}\langle 0,\ 0.7864,\ \bar{1}\rangle$, Type I-2$\{1\ \bar{1}\ 0\}\langle 1\ 1\ 2.7008\rangle$ and Type II-1 $\{0.7205,\ 0,\ \bar{1}\}\langle 010\rangle$, Type II-2 $\{1,\ 1,\ 3.0495\}\langle \bar{1}10\rangle$. The corresponding solutions of $\mathbf{b}$ and $\mathbf{m}$ in equation (15) are

$$\mathbf{b} = \rho\left(\sqrt{\frac{\lambda_3(\lambda_2 - \lambda_1)}{\lambda_3 - \lambda_1}}\mathbf{e}_1 + \kappa\sqrt{\frac{\lambda_1(\lambda_3 - \lambda_2)}{\lambda_3 - \lambda_1}}\mathbf{e}_3\right) \tag{18}$$

$$\mathbf{m} = \rho^{-1}\left(\frac{\sqrt{\lambda_3} - \sqrt{\lambda_1}}{\sqrt{\lambda_3 - \lambda_1}}\right)\left(-\sqrt{\lambda_2 - \lambda_1}\mathbf{e}_1 + \kappa\sqrt{\lambda_3 - \lambda_2}\mathbf{e}_3\right) \tag{19}$$

The definitions of the parameters in equations (18) and (19) are similar to those in equations (11) and (12), only ρ is used to make $\mathbf{m}$ as a unit normal vector. Equations (18) and (19) also represent two sets of $(\mathbf{b}, \mathbf{m})$ because of $\kappa = \pm 1$.

Proposition 5 of Ref. [5] gives $\det(\mathbf{C}(f) - \mathbf{I}) = \det(\mathbf{C}(1-f) - \mathbf{I})$, that is, if f is a solution of equation (17), $1-f$ is also a solution of equation (17). Generally matrices $\mathbf{C}(f)$ and $\mathbf{C}(1-f)$ have different eigenvalues and eigenvectors. Therefore, for each twin (corresponding to a pair of $(\mathbf{a}, \mathbf{n})$) we get two solutions of f from equation (17). For each volume fraction f, two sets of $(\mathbf{b}, \mathbf{m})$ are obtained from equation (18) and equation (19) for $\kappa = \pm 1$. So the total number of habit plane variants are $48 \times 2 \times 2 = 192$. For the Type II-1 case, the $\mathbf{b}$, $\mathbf{m}$ vectors are $\langle 0.0568,\ 0.0637,\ 0.0991\rangle$ and $\{0.8889,\ 0.4044,\ 0.2152\}$, respectively.

Once the habit plane orientations and the transformation strains are determined, it is possible to establish the transformation strain as,

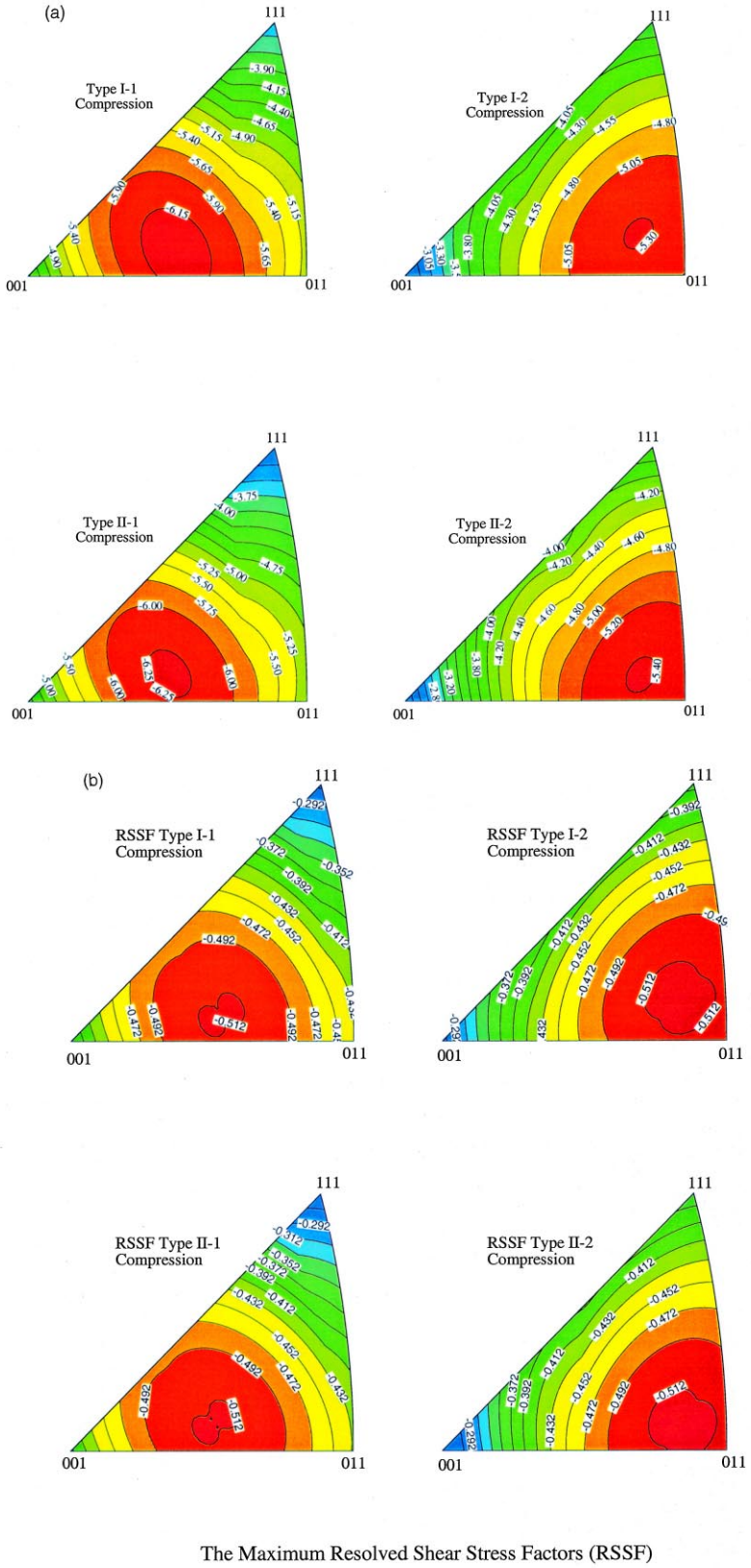

Fig. 8. (a) Equivalent transformation strain contours under compressive loading for the four twin types. (b) The resolved shear stress factor contours for four twinning types in compression.

Table 2. Calculated CVP strains and CVP + detwinning strains under different compressive loads for the four orientations studied in this work based on the energy minimization theory (see text for details)

	⟨112⟩				⟨148⟩				⟨001⟩				⟨111⟩			
	RSSF factor	Active CVPs	CVP strain (%)	CVP and detwin strain (%)	RSSF factor	Active CVPs	CVP strain (%)	CVP and detwin strain (%)	RSSF factor	Active CVPs	CVP strain (%)	CVP and detwin strain (%)	RSSF factor	Active CVPs	CVP strain (%)	CVP and detwin strain (%)
Type I-1 $f = 0.292$	0.444	(9,11) (9,12)	5.23	5.61	0.513	(9,12)	6.22	6.36	0.369	(9,11) (11,9) (9,12) (12,9) (10,11) (11,10) (10,12) (12,10)	4.09	4.09	0.267	(3,1) (4,1) (7,5) (8,5) (11,9) (12,9)	3.2	3.58
Type I-2 $f = 0.320$	0.387	(3,11) (7,12)	3.96	3.96	0.491	(12,7)	4.98	5.84	0.262	(9,1) (12,2) (11,3) (10,4) (9,5) (12,7) (10,8)	2.46	4.09	0.364	(3,11) (11,3) (4,8) (8,4) (7,12) (12,7)	3.58	3.58
Type II-1 $f = 0.271$	0.439	(9,11) (9,12)	5.14	5.61	0.512	(9,12)	6.24	6.36	0.386	(9,11) (11,9) (9,12) (12,9) (10,11) (11,10) (10,12) (12,10)	4.38	4.38	0.253	(3,1) (4,1) (7,5) (8,5) (11,9) (12,9)	2.98	3.58
Type II-2 $f = 0.323$	0.383	(9,1) (9,5)	3.97	5.61	0.478	(9,5)	4.99	6.36	0.223	(9,1) (12,2) (11,3) (10,4) (9,5) (12,7) (10,8)	1.99	4.09	0.356	(3,11) (11,3) (4,8) (8,4) (7,12) (12,7)	3.61	3.58

$$\varepsilon = \frac{1}{2}(\mathbf{F}_M^T \cdot \mathbf{F}_M - \mathbf{I})$$

$$= \frac{1}{2}[\mathbf{b} \otimes \mathbf{m} + \mathbf{m} \otimes \mathbf{b} + (\mathbf{b} \cdot \mathbf{b})\mathbf{m} \otimes \mathbf{m}] \quad (20)$$

In equations (18) and (20), $\mathbf{b}$ is not a unit vector and includes the shear magnitude, $|\mathbf{b}|$. Note that equation (20) differs from the small strain formulation which is given as

$$\varepsilon = \frac{1}{2}(\mathbf{F}_M + \mathbf{F}_M^T) - \mathbf{I} = \frac{1}{2}(\mathbf{b} \otimes \mathbf{m} + \mathbf{m} \otimes \mathbf{b}). \quad (21)$$

The small deformation theory produces recoverable strains which are approximately 10% higher (for compression) than the large deformation theory (Green strain) used in equation (20). The transformation strain results of the energy minimization theory are given in Fig. 8(a) using equation (20). The equivalent transformation strain contours are shown for all possible solutions on a standard (001) stereographic triangle. The contours are placed in 0.25% strain increments. We note that the transformation strain results obtained for the Type II-1 and Type I-1 twinning cases are not identical.

The detwinning strain (conversion of the small volume fraction variant to the large one within the CVP) can be determined as follows. From equation (14), variant $\mathbf{U}_j$ converts to $\mathbf{U}_i$ if volume fraction $f < 0.5$, and the deformation after detwinning is (by setting $f = 0$)

$$\mathbf{F}_M^{dt} = \mathbf{R}_h \mathbf{U}_i \quad (22)$$

If the volume fraction f is greater than 0.5, variant $\mathbf{U}_i$ converts to $\mathbf{U}_j$ and the transformation including detwinning is given by setting $f = 1$ as

$$\mathbf{F}_M^{dt} = \mathbf{R}_h \mathbf{R}_{ij} \mathbf{U}_j = \mathbf{R}_h \cdot (\mathbf{U}_i + \mathbf{a} \otimes \mathbf{n}). \quad (23)$$

Once $\mathbf{F}_M^{dt}$ is known the transformation strain (including CVP formation and detwinning) can be determined similar to equation (20) with $\mathbf{F}_M$ replaced by $\mathbf{F}_M^{dt}$. The results for CVP strains (in the absence of detwinning) and those with detwinning are presented in Table 2 for the orientations studied in this paper. The detwinning strain is as high as 0.6% in the ⟨111⟩ orientation. The focus is on the four orientations studied in this work. The active CVPs for each orientation are also provided in Table 2 as well as the resolved shear stress factor (RSSF) for all twinning types.

The resolved shear stress factor, RSSF, is simply defined as,

$$\text{RSSF} = (\mathbf{b} \cdot \mathbf{e})(\mathbf{m} \cdot \mathbf{e}) / |\mathbf{b}| \quad (24)$$

where $\mathbf{e}$ denotes the crystallographic direction of interest. The contour plots for the RSSFs in compression are provided in Fig. 8(b). We note that the location of the maximum resolved shear stress factor changes depending on the type of twinning. To

our knowledge, this is the first time where such a complete representation of theoretical results is provided for the NiTi alloy system.

4.3. Lattice deformation theory

Another approach, the so-called lattice deformation model, calculates the recoverable strain levels by directly considering the 12 lattice correspondences between the martensite and the austenite phase [4, 8]. The model assumes that the parent phase transforms into a single crystal of martensite without first forming a plate containing two twin-related martensite crystals (a CVP). To calculate the recoverable strain levels, the model first determines the local deformation gradient. Using calculations based on the correspondent variants, the maximum recoverable strain for the nickel–titanium alloy is then predicted. The parent phase of nickel–titanium is a B2 structure, which can be transformed into martensite with a B19′ structure.

The differences between this model and the first two presented above are as follows: the lattice deformation theory does not utilize the notion of habit plane and transformation shears: it uses a different rotation tensor and also does not account for the existence of an internal twin structure. The recoverable strains obtained from this theory are listed in Table 4 and also previously in Ref. [8] for the [001] and [111] orientations.

5. EXPERIMENTALLY DETERMINED RECOVERABLE STRAINS AND CRITICAL STRESSES

A large experimental program is undertaken examining four orientations and two heat treatments per orientation. A number of tests were repeated with consistent findings. The experimentally obtained stress–strain curves for [112] and [148] orientations are shown in Figs 9–10 and 11–12, respectively. For each orientation the stress–strain curve is accompanied by the recoverable strain as a function of increasing strain (shown with data points). We first discuss the behavior of [112] crystal in the over-aged condition. The strain in compression was increased from 2% to 7.5% in seven cycles (cycles 1–7 are marked on the figure). The specimen was heated after each cycle at zero stress to a temperature above A_f to realize the maximum recoverable strain before proceeding with the next cycle. The recoverable strain has two components: pseudoelastic strain and the shape memory strain. The pseudoelastic strain is associated with the reverse transformation (martensite to austenite) during unloading to zero stress (the PE effect). The shape memory strain is the further transformation of remaining austenite to martensite upon heating above A_f at zero stress (the SME effect). The recoverable strain is obtained from the total strain by removing the elastic and inelastic strain components (see Fig. 5).

The results in Fig. 9 exhibit three different regimes of deformation consistent with Fig. 5. The recoverable strains are shown with the data points in Fig. 9. It is worthwhile to note that the recoverable strain increases with increasing applied strain during Stage II. During Stage II the material can be

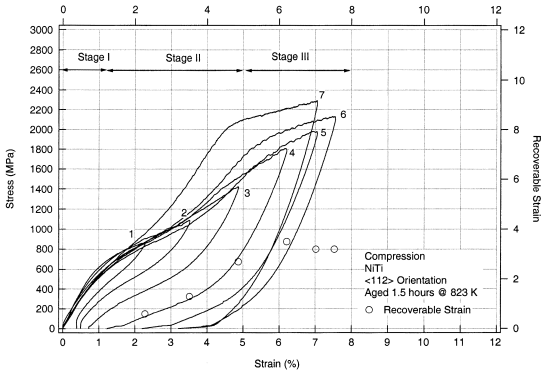

Fig. 9. The stress–strain response and recoverable strains (data points) for ⟨112⟩ case in the over-aged condition. Open symbols indicate recoverable strains.

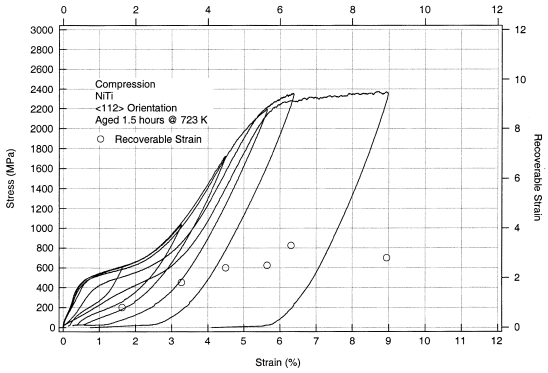

Fig. 10. The stress–strain response and recoverable strains (data points) for ⟨112⟩ case in the peak-aged condition.

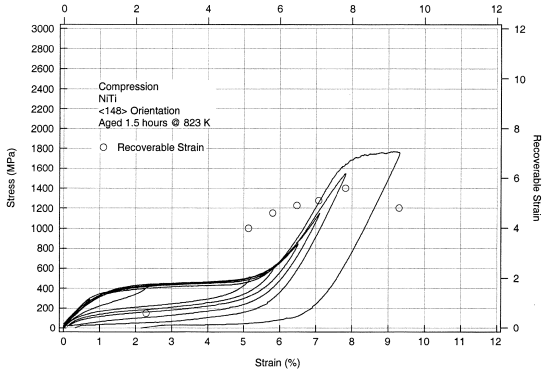

Fig. 11. The stress–strain response and recoverable strains (data points) for ⟨148⟩ case in the over-aged condition.

treated as a dual phase structure with additional hardening due to interaction of CVPs and blockage of further transformation by existing martensite boundaries. Hence the stress required to continue the transformation rises. In Stage III plastic deformation of martensite occurs producing a decrease in the stress–strain slopes. Martensite yielding can be estimated as the point of transition of the stress–strain slope form one of upward to downward curvature. In this case, martensite yielding occurred near 1700 MPa. The additional hardening of the martensite with cycling is consistent with the plastic deformation of the martensite and the build-up of dislocation structure.

Several observations are noteworthy on the recoverability of the strains. At small strains ($<2\%$) the transformation is purely pseudoelastic. However, as the applied strain increases the specimen was heated to 350 K (under zero stress) to allow unconstrained recovery of the strains (the SME effect). The RSSF factor for transformation have been determined and are summarized in Table 3. The RSSF factor corresponds to the CVP which will first undergo transformation. The theoretical results (Table 2) showed that more than one CVP exhibits the same RSSF factor in some of the orientations. The CRSS in Table 3 are determined as the product of RSSF factor and the critical transformation stress (0.2% offset). We note from Table 3 that the CRSS values for the over-aged case are consistently higher than the peak-aged case and the CRSS values are also orientation dependent. For the over-aged case the CRSS varies from 170 to 301 and the variation is 132–226 MPa for the peak-aged case.

The summary of theoretical predictions of the transformation strain and the experimentally measured recoverable strains are compared in Table 4. The recoverable strain observed in the experiments are consistently lower than the theoretical predictions. Only in the [148] and [001] cases the experimental recoverable strains approach the theoretical values.

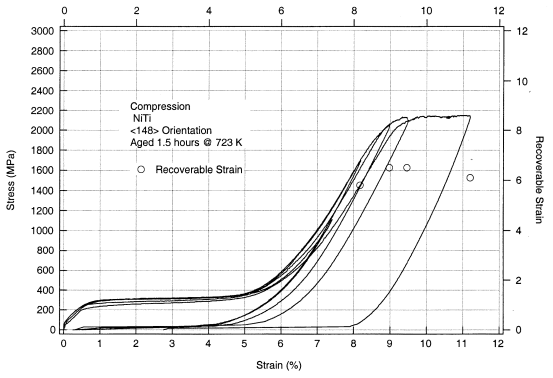

Fig. 12. The stress–strain response and recoverable strains (data points) for ⟨148⟩ case in the peak-aged condition.

Table 3. Summary of experimental results for the RSSF factor and the critical stress levels for austenite to martensite transformation (this study)

Crystal orientation	RSSF factor, compression		Experimental—critical uniaxial stress (MPa)+approx. values, compression		Experimental CRSS (MPa)	
	Phenomenological theory [2, 3] (Type II-1 twinning)	Energy minimization theory	Peak-aged	Over-aged	Peak-aged	Over-aged
[100]	0.4	0.39	330	485	132	194
[111]	0.27	0.25	551	874	138	219
[112]	0.39	0.44	514	685	226	301
[148]	0.49	0.51	283	334	144	170

Table 4. Summary of theoretical predictions of the transformation strain and the experimental recoverable strain levels for the four orientations studied in this work

Crystal orientation	Martensite formation strain			Experimental, recoverable strain, compression		
	Phenomeological theory [2, 3]	Energy minimization theory	Lattice deformation theory [4]	Peak-aged 1 h, 723 K	Over-aged 1 h, 823 K	Over-aged, 15 h, 773 K [8]
[100]	5.2%	4.4%	4.2%	3.6%	4.2%	4.3%
[111]	3.5%	3.6%	3.7%	1.8%	2.5%	3.0%
[112]	5.0%	5.1%	5.8%	3.3%	3.5%	–
[148]	6.0%	6.2%	6.6%	6.5%	5.6%	–

The stress–strain response for the [112] orientation that have undergone peak-aging treatment is shown in Fig. 10. The coherent stress fields of the precipitates reduce the transformation stress from 685 MPa to 514 MPa. The martensite yield stress is higher compared to the over-aged case, while the recoverable strains are comparable to the over-aged case. The increase in martensite yield stress is due to barriers to slip deformation by the precipitates and in this case the fine precipitates produce a higher resistance to slip.

The results of incremental unidirectional strain experiments for the [148] orientation in the over-aged and peak-aged condition are given in Figs 11 and 12, respectively. This orientation was chosen because it has a high RSSF factor (nearly 0.513) which implies that the transformation stresses would be low and the recoverable strains would be high (since the vectors **b** and **m** are not exactly orthogonal and RSSF larger than 0.5 is possible). Indeed, the transformation stresses are 283 MPa and 334 MPa and the recoverable strains are 6.5% and 5.6% for the peak-aged and over-aged cases, respectively. We note that in the case of [148] orientation the number of CVPs that are activated is 1 (see Table 2), and this limits the interaction of different variants and the transformation occurs at nearly constant stress.

The results of incremental strain experiments for the [111] and [001] crystal orientations are given in Figs 13–16, respectively. The [111] orientation exhibits rather low transformation strains (1.8% for peak-aged case and 2.5% for over-aged case) compared to the theoretical estimates (3.6%). The main reason for this difference is attributed to the fact that this orientation has six CVPs and consequently significant hardening. The hardening results in early yielding of the austenite and martensite phases, thereby limiting the transformation. We note that the [111] peak-aged case test is repeated on companion specimens producing almost identical results (circle and triangular data points in Fig. 14).

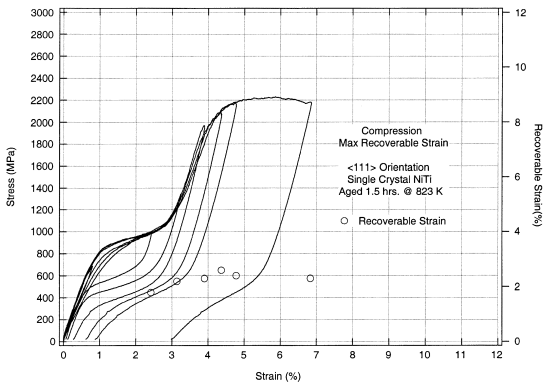

Fig. 13. The stress–strain response and recoverable strains (data points) for ⟨111⟩ case in the over-aged condition.

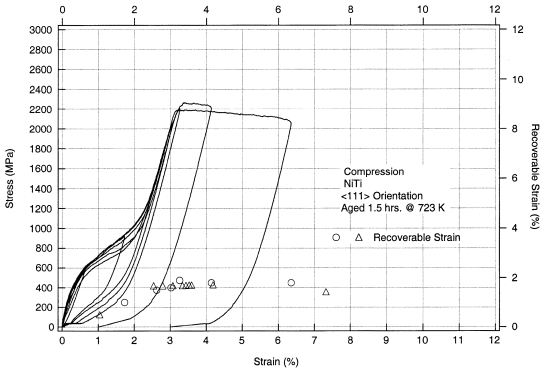

Fig. 14. The stress–strain response and recoverable strains for ⟨111⟩ case in the peak-aged condition. Open triangles and circles show recoverable strains on companion specimens, which were run in order to check repeatability of the tests.

The results for the [001] cases are presented in Figs 15 and 16 for the over-aged and peak-aged conditions, respectively. For each condition two tests have been conducted to check for repeatability of the results. In Fig. 15, the triangular data points and the circle data points are obtained from companion specimens. Figure 16 depicts the stress–strain and recoverable strain behavior of the [100] orientation in the peak-aged case. After austenite to martensite transformation, the austenite–martensite two phase microstructure behaves elastically with recoverable strain increasing during Stage II. In this orientation when the stress level reaches a critical level, fracture occurred. Again, the repeatability of the experimental results (the shape of the stress–strain curve, the recoverable strains, and the fracture ductility) is remarkable. To complete the interpretation of the results, the austenite yield levels in compression at room temperature are determined from Figs 3 and 4 and are listed in Table 5. The austenite yield levels are higher for the peak-aged case compared to the over-aged case. As expected, the austenite yield occurs in Stage II of the deformation. The Schmid factors for austenite slip are also listed in Table 5 (using {110}⟨100⟩ systems [13]) as well as the number of active slip systems.

To gain further insight into the results, the slip Schmid factors for the martensite that forms from austenite have been calculated. Since the orientations of the martensite CVPs are known with respect to the cubic axis the slip systems {110}⟨111⟩ were used to evaluate the Schmid factors. The Schmid factor for slip in the different CVPs that form are determined to be similar except for the [001] case. The results are summarized in Table 6. The number of slip systems in the [148] orientation is only 1, hence the single system produces very low levels of strain hardening in the martensite. The number of active slip systems for the [112] case is 2 with a Schmid factor of 0.47. In this case once martensite yielding occurs the stress–strain response exhibits considerable hardening. The results tabulated show that the martensite yield levels are nearly 2100 MPa in the peak-aged case, while they are approximately 1700 MPa for the over-aged case.

6. DISCUSSION OF RESULTS

The results show that the end of the stress plateau in the [148] orientation is not the end of the stress induced phase transformations in compression. The increase in the unloading modulus with deformation in Stage II lends further proof that the martensite volume fraction is increasing during the ascending portion of the stress–strain curve. Since the martensite modulus is higher than the austenite elastic modulus by a factor of two, the results correlate well with transformation during Stage II. The transformation also proceeds past the austenite yield stress (as determined from the stress-temperature plots, Figs 3 and 4). One reason why the transformation continues even after apparent yielding of austenite is that there exist residual austenite regions in the material. Bataillard *et al.* [10] have observed the nonhomogenous nature of the phase transformation at the local level by *in-situ*

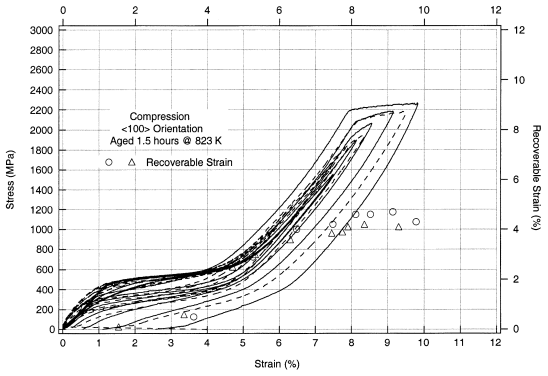

Fig. 15. The stress–strain response and recoverable strains (data points) for ⟨100⟩ case in the over-aged condition. The recoverable strain data are denoted by symbols.

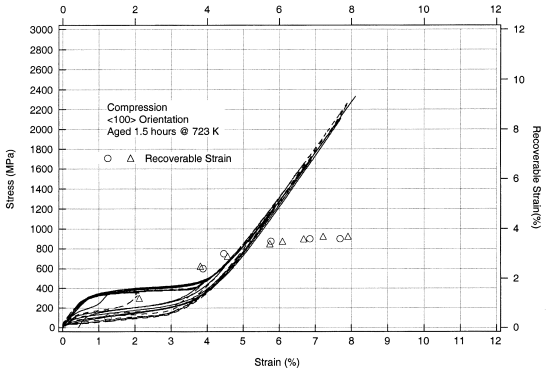

Fig. 16. The stress–strain response and recoverable strains (data points) for ⟨001⟩ case in the peak-aged condition.

Table 5. Schmid factors for the austenite and the experimentally determined yield stress levels for the four orientations (this study)

Crystal orientation	Schmid factor—Austenite {100}⟨110⟩	# of slip systems	Experimental, austenite yield stress (MPa) based on Figs 3 and 4	
			Peak-aged	Over-aged
[100]	0	–	[a]	[a]
[111]	0.47	2	1250	900
[112]	0.47	2	1200	950
[148]	0.35	2	1100	850

[a] Austenite yielding is ruled out.

transmission electron microscopy. Also, previous calculations [6, 7] show that selective transformation occurs near precipitates at locations where the applied shear stresses and the local shear stresses resolved on the most favorably oriented CVP reach a critical value. Only after yielding of martensite in Stage III, which is internally twinned in NiTi alloys, did the recoverable strains decrease with further deformation (Figs 9–16, Stage III). Apparently, the martensite structure is deformed enough where it cannot revert back to the austenite.

Although the stress–strain curves for the [148] orientation indicate a ''Luders'' type transformation propagation, there are many transformation interfaces forming in the precipitated crystals due to the very inhomogeneous microstructure. As the specimen strain is increased, new martensite plates are nucleated near precipitates. The presence of slip pile-ups at precipitates have been also observed. The presence of pile-ups have the role of increasing the slip resistance, hence hardening the matrix, at the same time generating considerable internal stresses. Precipitates prevent small local areas of the specimen from transforming back to the parent phase. The generation of more defects and the increase of local pile-up stresses leads to the observed increase in the transformation stress–strain slope during the deformation. Since local dislocation pile-ups are observed in TEM study of the samples (Fig. 2), the internal stresses from the pile-ups are believed to contribute to the nonlinear unloading response. The nonlinearity upon unloading is most pronounced in Stage II where the material is a two phase mixture of austenite and martensite and significant internal stresses are present. The role of the internal stresses is to limit the damping capacity (hence hysteresis) in these alloys.

The decrease in transformation stress upon peak-aging can be readily linked to the coherent stress fields (Table 3). When coherent or semi-coherent precipitates are formed a strong local stress field is developed in the NiTi matrix due to the mismatch in lattice parameters of the precipitates vs the matrix. The local stress fields result in local resolved shear stresses on the martensite CVPs, and thus create preferential nucleation sites for the martensitic transformation. To estimate the effect of the local stresses on the martensitic transformation, the local stress fields outside of the precipitate are resolved onto the 24 martensite correspondence variant pairs (CVPs). The local resolved shear stresses are extremely large on some CVPs and negligible on others. Calculations of such stress fields confirmed that the critical resolved shear stresses resolved into the most favorable CVP were in the range 50–150 MPa [6, 7] consistent with the results shown in Table 3. This difference in local stress readily explains the variation in critical transformation stress levels in Table 3.

The primary difference between the [148] and other orientations is that the other orientations lie on a symmetry boundary, while the [148] orientation lies within the stereographic triangle. Because of this, the [148] has one CVP favored for transformation (Table 2). The multiplicity of martensite CVPs leads to more drastic effects in incremental loading in the [112], [001] and [111] orientations. Specifically, the interaction of multiple slip systems and martensite plates leads to a quicker generation of damaging defects. The variant–variant interaction effect has been modeled in the past through an interaction matrix and is similar to latent hardening in slip induced deformation [9, 14]. The role of the multiple CVP in-

Table 6. Calculated Schmid factors, number of slip systems for the martensite formed and the experimental yield values for the martensite (this study)

Crystal orientation	Schmid factor martensite	# of slip systems	Experimental, martensite yield stress (MPa) + approx. values	
			Peak-aged	Over-aged
[100]	0.40	8	Brittle fracture	1700
[111]	0.47	2	2100	1700
[112]	0.47	2	2100	1700
[148]	0.48	1	2000	1500

teractions is to produce an ascending stress–strain curve rather than a stress plateau typically identified with SMA alloys.

The strength of the martensitic structure achieved at the conclusion of the transformation is strongly dependent on the precipitate size and spacing. Peak-aging produces strength levels nearly 500 MPa higher than the over-aged case. The increased martensite yield stress is beneficial in extending the regime where austenite to martensite transformation proceeds (Stage II). Van Humbeeck and colleagues [15, 16] found that under tension of martensite structure ($T < M_f$) two accommodating variants change to one variant favorable to stress. This results in reorientation of martensite as further detwinning develops. In this case martensite plates containing ⟨011⟩ Type II twins are twin related with a junction plane ⟨001⟩ which migrates under tensile deformation. In contrast, under compression, this mechanism was not favored and deformation occurred through generation of high density of dislocations both inside the martensite twins and the junction planes [15, 16].

The calculations for the Schmid factors of the austenite and martensite phases were useful (Tables 5 and 6) as they pointed out the lowest Schmid factors for the [001] case resulting in increased recoverable strains in this orientation. Austenite yielding is not expected in this orientation due to the prevailing ⟨100⟩{110} slip system [13]. The yield stress vs temperature results given in Figs 3 and 4 confirm the remarkable resistance to slip in the [001] direction. In the incremental strain experiments, the maximum recoverable strain coincided with the critical stress for martensite yielding. Once the stresses exceed this critical stress, the recoverable strains decrease with increasing strain. Therefore, any treatments that increase the martensite flow stress would increase the transformation strain.

The yield stress results for the B2 phase at high temperatures were used to determine the yield stress of austenite for slip at lower temperatures. At room temperature, this is done by linear extrapolation of the high temperature results. It was found that the yield strength for slip for the ⟨112⟩ case and ⟨148⟩ case are comparable (Table 5), but the slip of austenite occurs at much higher strains for the ⟨148⟩ case compared to the ⟨112⟩ case. This behavior is expected because the critical stress for $A \rightarrow M$ transformation is substantially lower for the [148] case (Table 3). These results can be used to note why the recoverable strains are considerably higher for the ⟨148⟩ case compared to the ⟨112⟩ case. Another important observation is that peak-aging increases the M_d temperature by nearly 60 K compared with over-aged crystals. Therefore, the deformation temperature relative to the M_d temperature is an important consideration in interpretation of the results. Thermomechanical treatments such as ausforming have been suggested to increase the strength of the austenite phase thereby extending the region of transformation.

7. CONCLUSIONS

The work supports the following conclusions:

1. The end of the stress plateau is not the end of the austenite to martensite transformation. The austenite to martensite transformation continues beyond the stress plateau and during the ascending portion of the stress–strain curves until the yield strength of martensite is reached. TEM observations were made to support that the deformation patterns around the precipitates are not homogenous resulting in local untransformed areas which gradually transform with increasing remote strain.
2. In two of the orientations studied ([112], [111]) multiple CVPs are activated leading to rapid hardening in the stress–strain response. The outcome of the higher hardening rates is to reach austenite and martensite critical stresses for slip, thereby limiting the overall transformation strain. Only in the [148] case a single CVP is activated and transformation occurs over a plateau stress with recoverable strains reaching theoretical values. In the [001] case, the austenite exhibits no plastic flow allowing high transformation strains prior to brittle fracture.
3. The theoretical calculations for the transformation strains were made using the energy minimization theory modified to account for detwinning effects and large strain deformation. The predictions presented here are more complete and accurate than previous work by the authors which relied on the phenomenological and lattice deformation theories. These comparisons are provided in the paper for completeness. Type II-1 twinning produces the highest transformation strains in compression with the Type I-1 twinning solution producing slightly smaller transformation strains. The model correctly predicts that in compression the [148] orientation produces the highest transformation strains, while the [111] orientation delivers the smallest transformation strains.
4. The results point out that any treatments or orientation control that increase the strength of austenite and martensite phases will delay slip and permit the recoverable strains to reach theoretical values. Since the slip in B2 phase is strongly orientation dependent, the [001] and [148] orientations with the lowest Schmid factors for austenite slip produced the highest recoverable strains. In addition, the increase in austenite strength via peak-aging has been measured through the increase in the M_d temperature. Therefore, processes such as ausforming for

strengthening the austenite can be utilized to raise the recoverable strain levels.

5. The [001] orientation, which is least favorably oriented for slip, exhibits a dramatic increase in yield stress with increasing temperature. This orientation also displays the smallest inelastic strains with deformation as shown in this work. This results in experimental transformation strain levels similar to the theoretical prediction of 4.4%.

Acknowledgements—The research is supported by a grant from the Department of Energy, Basic Energy Sciences Division, Germantown, Maryland, DOE DEFG02-93ER14393. Additional support was obtained from the National Science Foundation contract CMS 99-00090, Mechanics and Materials Program, Arlington, Virginia. Professor Chumlyakov received support from the Russian Fund for Basic Researches, Grant Nos. 02-95-00350, 99-03-32579. The facilities at Microanalysis of Materials, Materials Research Laboratory were used. This laboratory is funded by DOE-DMS grant DEFG02-96ER45439.

REFERENCES

1. Otsuka, K. and Wayman, C. M., *Shape Memory Materials*. Cambridge University Press, Cambridge, 1998.
2. Wechsler, M. S., Lieberman, D. S. and Read, T. A., *Trans. AIME*, 1953, **197**, 1503.
3. Buchheit, T. E. and Wert, J. A., *Metal. Trans.*, 1996, **27A**, 269.
4. Saburi, I. and Nenno, S., *Proc. Int. Conf. Solid–Solid Phase Transf., Pittsburgh,* 1981, pp. 1455–1479.
5. Ball, J. M. and James, R. D., *Arch. Rat. Mech. Anal.*, 1987, **100**, 13.
6. Gall, K., Sehitoglu, H., Chumlyakov, Y. I., Kireeva, I. V. and Maier, H. J., *J. Engng Mater. Technol.*, 1999, **121**, 19.
7. Gall, K., Sehitoglu, H., Chumlyakov, Y. I., Kireeva, I. V. and Maier, H. J., *J. Engng Mater. Technol.*, 1999, **121**, 28.
8. Gall, K., Sehitoglu, H., Chumlyakov, Y. and Kireeva, I., *Acta mater.*, 1999, **47**(4), 1203.
9. Gall, K. and Sehitoglu, H., *Int. J. Plasticity*, 1999, **15**, 69.
10. Bataillard, L., Bidaux, J. E. and Gotthardt, R., *Philos. Mag. A.*, 1998, **78**(2), 327.
11. Matsumoto, O., Miyasaki, M., Otsuka, K. and Tamura, H., *Acta metall.*, 1987, **35**, 2137.
12. Hane, K. F. and Shield, T. W., *Philos. Mag. A*, 1998, **78**, 1215.
13. Chumlyakov, Y., Surikova, N. S. and Korotaev, A. D., *Phys. Metal. Metallogr.*, 1996, **82**(1), 102.
14. Patoor, E., Siredey, N., Eberhardt, A. and Berveiller, M., *J. Phys. III*, 1995, **5**(C8), 227.
15. Xie, Z., Liu, Y. and Van Humbeeck, J., *Acta mater.*, 1998, **46**(6), 1989.
16. Liu, Y., Xie, Z. L., Van Humbeeck, J. and Dealey, L., *Acta mater.*, 1999, **47**(2), 645.